JN-RM-1169-24

Synaptic Vesicle Glycoprotein 2A Knockout in Parvalbumin and Somatostatin Interneurons Drives Seizures in the Postnatal Mouse Brain

Odile Bartholome, Virginie Neirinckx, Orianne De La Brassinne, Jana Desloovere, Priscilla Van Den Ackerveken, Robrecht Raedt, and Bernard Rogister

QUERY SHEET

This page lists questions we have about your paper. The numbers displayed at left are hyperlinked to the locations of the queries in your paper.

The title and author names are listed on this sheet as they will be published, both on your paper and on the Table of Contents. Please review and ensure the information is correct and advise us if any changes need to be made. In addition, please review your paper as a whole for typographical and essential corrections.

Your PDF proof has been enabled so that you can comment on the proof directly using Adobe Acrobat.

Using your cursor, select the text for correction, right click, and use the most appropriate single tool (i.e., "Replace," "Cross out," or "Add note to text"). To insert, place the cursor, then go to Tools/Comment and Mark up/Text edits/Insert text at cursor.

In case of difficulty, please use the "Sticky note" function.

The CrossRef database (www.crossref.org/) and PubMed database (https://pubmed.ncbi.nlm.nih.gov/) have been used to validate the references.

AUTHOR QUERIES

QUERY NO.	QUERY DETAILS
AQ1	Headings have been updated per journal style. Please check the heading hierarchy and make any changes directly in the text.
AQ2	As per style guide, the use of italics for emphasis is not permitted. Hence, all occurrence of italicized text has been changed to roman and enclosed in double quotation marks. Please check and correct if necessary.
AQ3	The duplicate entry of the "Bartholome et al., 2020, Goebbels et al., 2006, Lynch et al., 2004, Tronche et al., 1999" has been removed from the reference list. Please check.
AQ4	Please provide missing DOI, if available, for the "Bartholome et al., 2020, Miri et al., 2018, Pfisterer et al., 2020, Serrano et al., 2019, Tai et al., 2014 and Vanoye-Carloa and Gómez-Lirab, 2019" references list entry.
AQ5	Please provide missing page number for the "Keller et al., 2018, Miri et al., 2018, Pfisterer et al., 2020, Serrano et al., 2019 and Tai et al., 2014" references list entry.
AQ6	Please provide missing Journal title for the "Pack, 2024" references list entry.
AQ7	Please provide the in-text citations for Extended Data 2-1, 2-2, 3-1, 5-1, 5-2, 7-1.

QUERY NO.	QUERY DETAILS
AQ8	Upon checking, it was noticed that there is citation of panel label D in the image of Fig. 6; however, it was missing in the corresponding caption. Please check and ensure that panel labels within the figure caption correspond with the image.

Neurobiology of Disease

Synaptic Vesicle Glycoprotein 2A Knockout in Parvalbumin and Somatostatin Interneurons Drives Seizures in the Postnatal Mouse Brain

Odile Bartholome,[1] Virginie Neirinckx,[1] Orianne De La Brassinne,[1] Jana Desloovere,[2] Priscilla Van Den Ackerveken,[1] Robrecht Raedt,[2] and Bernard Rogister[1,3]

[1]Nervous System Disorders and Therapy, GIGA Institute, University of Liège, Liège 4000, Belgium, [2]Brain Lab, Ghent University, Ghent 9000 Belgium, and [3]Neurology Department, CHU, Academic Hospital, University of Liège, Liège 4000 Belgium

Synaptic vesicle glycoprotein 2A (SV2A) is a presynaptic protein targeted by the antiseizure drug levetiracetam. One or more of the three SV2 genes is expressed in all neurons and is essential to normal neurotransmission. Loss of SV2A results in a seizure phenotype in mice and mutations in humans are also linked to congenital seizures. How SV2A action impacts the epileptic phenotype remains unclear, especially among the diverse neuronal populations that regulate network excitability. This study explored how brain structure and function are affected by SV2A conditional knock-out (SV2A-cKO) in specific neural cell subtypes. We show that SV2A-cKO in all neurons of the postnatal brain triggers lethal seizures, suggesting that the seizures observed in earlier knock-out models were not due to aberrant brain development. Similar lethal seizures are detected in mice in which the loss of SV2A is limited to GABAergic neurons, whereas loss in excitatory neurons produces no noticeable phenotype. No apparent gender difference was ever observed. Further investigation revealed that SV2A-cKO in different GABAergic interneuron populations induces seizure, with variable timescales and severity. Most notably SV2A-cKO in parvalbumin interneurons (PV^+) leads to lethal seizures in young animals, while SV2A-cKO in somatostatin (SST) inhibitory neurons results in seizures that were scarcely observed only in adult mice. These results support the crucial role SV2A plays in PV and SST interneurons and suggest that the action of levetiracetam may be due largely to effects on a subset of GABAergic interneurons.

Key words: **brain development and maturation; epilepsy; GABAergic interneurons; SV2A**

Significance Statement

The synaptic vesicle glycoprotein 2A is the target of the antiseizure drug levetiracetam, and the SV2A full knock-out in mice induces severe seizures. Still, SV2A function in synapses is yet not fully elucidated, including the neuronal subtypes in which SV2A expression is mandatory or dispensable. In this paper, we demonstrated that SV2A knock-out in inhibitory neurons provokes seizure (including PV^+ and SST^+) whereas it does not induce any visible phenotype in excitatory neurons. Our study supports the key role of SV2A in interneuron populations, in the context of epilepsy.

Introduction

Epilepsy is a chronic brain pathology that has been a major health burden for centuries. It nowadays affects over 45 million people worldwide (Beghi et al., 2019), yet its physiopathology remains poorly understood. This disease is characterized by spontaneous seizure, caused by abnormal or synchronous neuronal firing resulting from a global imbalance in excitatory and inhibitory processes. Hypersynchronous EEG discharges entail the abnormal activity of glutamatergic neurons that were long considered the first-line culprits. Yet, inhibitory neurons (GABAergic, interneurons) have later been appointed as key actors in ictogenesis, displaying a high-frequency firing pattern at seizure onset that further affects excitatory neuron activity (Grasse et al., 2013; Librizzi et al., 2017; Elahian et al., 2018) However, questions remain about

Received June 19, 2024; revised Nov. 15, 2024; accepted Dec. 10, 2024.

Author contributions: O.B., V.N., P.V.D.A, and B.R. designed research; O.B., V.N., O.D.L.B., J.D., P.V.D.A., R.R., and B.R. performed research; B.R. contributed unpublished reagents/analytic tools; O.B., V.N., J.D., P.V.D.A., and R.R. analyzed data; V.N. and B.R. wrote the paper.

We thank Dr. Dominique Baiwir and Dr. Gabriel Mazuchelli from the GIGA-Proteomics Core Facility for their valuable help in the mass spectrometry analysis. The microscopy images were acquired with the support of Dr. Sandra Ormenese and the GIGA-Cell Imaging facility. We thank Benoît Brouwers, Thérèse Aldenhoff, and Lien De Schaepmeester for the technical assistance. This study was supported by Fonds De La Recherche Scientifique–FNRS and Fonds Wetenschappelijk Onderzoek.

The authors declare no competing financial interests.

Correspondence should be addressed to Bernard Rogister at Bernard.Rogister@uliege.be.

https://doi.org/10.1523/JNEUROSCI.1169-24.2024

which interneuron networks are involved or about the dynamics of the interplay between excitatory and inhibitory neurons during seizure initiation and evolution (Dossi and Huberfeld, 2023). Understanding the molecular determinants of interneuron activity is therefore highly relevant for paving the way toward their therapeutic modulation to possibly regulate seizure.

Interestingly, among other peculiarities, increasing evidence highlights that inhibitory neurons express higher amounts of the synaptic vesicle glycoprotein 2A (SV2A; Tokudome et al., 2016; Vanoye-Carloa and Gómez-Lirab, 2019; Bae et al., 2020; Pazarlar et al., 2022). This protein belongs to the SV2 family and is found in the brain and endocrine tissue and in the membrane of neuronal and endocrine vesicles (Portela-Gomes et al., 2000). Among the three SV2 isoforms reported in mammals, *SV2A* is ubiquitously and highly expressed in all neurons of the brain. *SV2B* is found in excitatory neurons in most brain regions, while *SV2C* expression is essentially restricted to specific neuronal subpopulations (Bajjalieh et al., 1994; Pazarlar et al., 2022). SV2A has been appointed as a key player in neurotransmission, since SV2A knock-out (SV2A-KO) mice were shown to experience severe seizure, leading to death between postnatal days 7 and 21. SV2A-KO animals presented abnormal postsynaptic currents (PSCs) while conserving a normal brain architecture (Crowder et al., 1999; Janz et al., 1999, Venkatesan et al., 2012). On the contrary, SV2B-KO mice do not exhibit seizures (Janz et al., 1999). Later, the antiseizure drugs (ASDs) levetiracetam and its derivatives (e.g., brivaracetam) were identified as SV2A modulators (Lynch et al., 2004). These ASDs effectively suppress seizure in a wide range of epilepsies and are well tolerated and safely combined with other medications (Pack, 2014; Löscher et al., 2016).

At the molecular level, SV2A interacts with synaptotagmin 1 (Syt1) to ensure Syt1 recycling and slows down endocytosis of synaptic vesicles (Schivell et al., 1996; Schivell et al., 2005; Kaempf et al., 2015; Bae et al., 2020). However, in vitro experiments showed that rescuing the normal concentration and location of Syt1 in SV2A-KO neurons does not restore normal PSCs (Nowack et al., 2010), suggesting that the loss of Syt1 interaction is not sufficient to explain the neurotransmission defects observed in the SV2A-KO mouse. The complete spectrum of SV2A functions therefore remains to be elucidated.

In our paper, we aimed to shed light on the function that SV2A could play in seizure, by knocking it out from specific neuronal populations in the adult brain. We used genetically modified, Cre-lox-based mouse models to investigate the consequences of *SV2A* deficiency in different neuronal subtypes. Different mouse lines expressing Cre-recombinase in specific cell types were crossed with SV2A lox/lox mice to induce recombination of the *SV2A* gene, leading to a truncated, unfunctional SV2A protein (Menten-Dedoyart et al., 2016). This allowed us to study the functional consequences of SV2A deficiency at the level of the whole organism (Ubc:SV2A-cKO), all neurons (Nes:SV2A-cKO), excitatory neurons (Nex:SV2A-cKO), or distinct populations of inhibitory neurons (Dlx:SV2A-cKO, PV:SV2A-cKO, SST:SV2A-cKO, VIP:SV2A-cKO). Whereas no phenotype was recorded upon SV2A deficiency in glutamatergic neurons, mice developed seizures upon SV2A invalidation in inhibitory neurons, especially in parvalbumin (PV) or somatostatin (SST) interneurons. The SV2A invalidation in PV neurons induces lethal epileptic activity in early life, while invalidation in SST^{+} neurons results in seizure activity only at adult age. Animals with seizures demonstrated reduced body weight, but no major change in brain structure or neuronal density. We also observed an altered brain electrical activity at the electroencephalogram (EEG) in PV:SV2A-cKO and SST:SV2A-cKO. Proteomic analyses of SV2A-deficient excitatory and inhibitory synaptosomes highlighted a panel of proteins that were found differentially expressed. Altogether, these findings suggest that a proper SV2A function in inhibitory interneurons is crucial to sustain physiological neurotransmission.

Material and Methods

Animals

Animals were bred and housed at the Central Animal Facility from the University of Liège and GIGA Institute. Both males and females were considered for our experiments. Animal care followed the declaration of Helsinki and the guidelines of the Belgium Ministry of Agriculture, in agreement with the European Community Laboratory Animal Care and Use Regulations. Experimental research on the animals was performed with the approval of the University of Liège ethics committee (Belgium), filed under number 1753, and accepted in 2016. AQ1

Conditional knock-out mice were obtained by crossing SV2A lox/lox mice (generated by Ozgene and previously validated (Löscher et al., 2016) and either UbiquitinC-creERT2 (Ubc-cre, JAX stock #007001), Nestin-cre [Nes-cre, JAX stock #003771 (Tronche et al., 1999)], Nex-cre [gracefully provided by Prof. Nave Klaus-Armin (Goebbels et al., 2006)], Dlx5.6-cre [Dlx-cre, JAX stock #023724 (Stenman et al., 2003)], PV-cre [JAX stock #012358 (Madisen et al., 2010)], and SST-cre or VIP-cre [JAX stock #018973 and #010908 (Taniguchi et al., 2011)]. All crossings were based on $cre^{+/-}$; $SV2A^{lox/+}$ males and $cre^{+/+}$; $SV2A^{lox/lox}$ females, except for the PV:SV2A mouse line that was maintained with crossing $cre^{+/-}$; $SV2A^{lox/+}$ females and $cre^{+/+}$; $SV2A^{lox/lox}$ males (due to the reported expression of PV in sperm cells). Besides, two cre-reporter constructs were used to visualize recombinant cells, namely, RosaR26R-yellow fluorescent protein [JAX stock #006148 (Srinivas et al., 2001)]. In this paper, all mutant mice (XXX-$cre^{+/-}$; $SV2A^{lox/lox}$) will be referred to as "XXX-cre:SV2A-cKO." Individuals with the genotype XXX-$cre^{+/+}$ are considered wild type (WT), whatever the status of the SV2A gene.

Tamoxifen induction

Ubc:SV2A-cKO mice and their associated WT littermates were treated for 5 d with tamoxifen (Sigma-Aldrich), dissolved at 30 mg/ml in a sunflower oil/ethanol (9:1) mixture to induce the recombination. The treatment was started at P70 and administered by "oral gavage" (180 mg/kg body weight/administration). AQ2

Animal monitoring and seizure assessment

Mice were monitored twice an hour per day to track seizure onset, based on the modified Racine scale (Van Erum et al., 2019). The duration of monitoring was adapted to the mouse line. We surveilled the animals from birth/induction until death. We observed seizures that were consistently displayed as sudden circle racing with wild jumping, before animals fell on their side in tonic–clonic movements, corresponding to a Racine score of 5. Mice either died in seizure during observation sessions (at least one mouse in each epileptic line) or were found dead in the cage the next morning. Mouse weight was recorded from birth/induction until death, and the presence of milk in the stomach was verified after death/sacrifice to ensure that all pups were eating. However, we can't rule out that the pups undergoing seizure eat a bit less, or at a lower frequency, resulting in a reduced body weight.

RNA extraction and quantitative real-time PCR

Total RNA was extracted from whole-brain tissue using TRIzol reagent (Invitrogen), treated with DNase I (Promega) prior to reverse transcription from 1 µg total RNA using M-MLV Reverse Transcriptase (Promega). The resulting first-strand cDNA was used for real-time PCR using a SYBR Green Master Mix (Roche) in a LightCycler 480 (Roche). At least three biological replicates were analyzed, in technical triplicates. Primer sequences were as follows: SV2A For: GTCTTT GTGGTGGGCTTTGT, Rev: CGAAGACGCTGTTGACTGAG; SV2B For: AAACGCGGTGAGCATCTTAG, Rev: ACTTCAGAGCCACCA

TGGAC; SV2C For: TCTTTGCCTTCCTCTCCTCA, Rev: GAACATGC AGAGCCAACTGA. Gene expression levels were normalized upon the glyceraldehyde-3-phosphate dehydrogenase (GAPDH) housekeeping gene.

Western blot analysis

Mice were killed by dislocation, and then the brain was rapidly dissected and frozen at −80°C. Whole-brain tissue was ground in lysis buffer (450 mM NaCl, 50 mM Tris-HCl, 1% Triton X-100, 1% protease and phosphatase inhibitor) and left for 15 min on ice. After 10 min of centrifugation at 10.000 × *g*, the supernatant is recovered, and protein content is measured using the Bradford assay. Depending on the experiment, 15 to 20 µg of proteins were mixed in 20 µl of loading buffer (62.50 mM Tris-HCl, 20% glycerol, 2% SDS, 0.01% bromophénol blue, 5% mercaptoethanol) and heated at 70°C for 10 min. After protein separation and transfer, the PVDF membrane was blocked for 1 h in TTBS with 5% AQ7 milk at RT. Primary antibodies (Extended Data Table 1-1) were diluted in the blocking buffer and incubated overnight at 4°C. Next, the membrane was immersed in the corresponding secondary antibody diluted at 1/5,000 in TTBS for 1 h at RT. HRP-conjugated anti–β-actin antibody was used at 1/10,000 for 1 h at RT. After TTBS washing, blots were incubated with ECL substrate (Pierce, Thermo Fisher Scientific), and chemiluminescent signals were recorded with ImageQuant camera (GE HealthCare) and ImageQuant software. Signals corresponding to SV2 proteins were normalized against β-actin signals, and results from the cKO individuals were later normalized to WT littermates.

Synaptosome analysis

Protein extraction from hippocampal synaptosome preparation. Mice were killed by dislocation. After brain extraction, both hippocampi were microdissected and directly frozen at −80°C. Samples were ground as whole homogenates (H) in an ice-cold Krebs buffer. After 10 min of centrifugation at 1,000 × *g*, cell pellet (P) was separated from the supernatant that was centrifuged again at 16,000 × *g* for 20 min to obtain a pellet of synaptosomes (S), which was then frozen at 80°C.

Mass spectrometry. The protein quantity of synaptosomes samples was evaluated using the kit RC/DC (Bio-Rad) according to the manufacturer's protocol after being resuspended in 100 µl of 10 mM Tris buffer, 1% SDS, pH7.4. Twenty micrograms of each sample were reduced using DTT, alkylated using iodoacetamide, and precipitated using a 2D clean-up kit (GE HealthCare). Samples were resuspended again at 0.5 µg/µl in ammonium bicarbonate 50 mM and digested with trypsin. Subsequently, 3.5 µg of digested proteins were purified (ZipTip C18), dried, and resuspended at 0.222 µg/µl in 100 mM ammonium formate.

Samples were injected on a nano 2D UPLC-Orbitrap MS system along with an internal standard for quality control. The 2D analysis was performed in positive ion mode by an LC-ESI quadrupole orbitrap (Q Exactive Plus, Thermo Fisher Scientific). Samples were diluted on a low-pH column and then separated on a high-pH column. The entire process consisted of an increasing concentration of acetonitrile. A TopN-MSMS performed the mass spectrometer quantification (label-free), and the software MaxQuant was used for database searches. Protein identification was considered significant with at least two peptides per protein, considering only an FDR of <0.01. An ANOVA analysis was carried out following a Tukey posttest, and the level of significance was set at $p < 0.05$ (Perseus software).

Immunostainings and histological analyses

Mice were killed with an intraperitoneal injection of Euthasol (450 mg/kg) followed by intracardiac perfusion of ice-cold saline solution (0.9% NaCl) and 4% paraformaldehyde (PFA) in PBS. Harvested brains were postfixed overnight at 4°C in PFA and then placed in PBS–sucrose 30% before being cut in 16-µm-thick cryosections. After toluidine blue staining of brain sections, cortical thickness was measured from the corpus callosum to the surface of the cortex. Three to four images, distributed across the brain, with a clear coronal vision of the whole encephalon were selected for each animal.

For immunolabelling, brain sections on glass slides were immersed in citrate buffer (Dako Target Retrieval Solution), heated, and then blocked with 10% normal donkey serum (NDS) in 0.3% PBS–Triton X-100, for 30 min at RT. Brain sections were then incubated overnight at 4°C with primary antibodies (Extended Data Table 1-1), in PBS supplemented with 1% NDS in 0.1% PBS–Triton X-100. The next day, slices were immersed in PBS with donkey secondary antibodies (Jackson ImmunoResearch), for 1 h at RT. After 5 min incubation with DAPI at RT, slices were finally mounted with Safe Mount. Images were acquired with an FV1000 (Olympus) or Nikon A1R (Nikon) confocal microscope. Negative control stainings (without primary antibodies) served in setting up a signal background and identifying immunoreactive cells. The rostral landmark corresponded to the somatosensory area (appearance of the hippocampi). The caudal landmark corresponded to the visual area (where the CA3 hippocampal region reaches the ventral part of the brain). For cortical cell density, positive cells were counted on each selected slice in a ROI drawn from the corpus callosum to the surface of the cortex. For hippocampal cell density, the whole hippocampus was drawn and measured. Three whole hippocampal sections were averaged for each animal. ROI drawing and blind counting were performed using ImageJ software.

RNAscope and BaseScope

For RNAscope and BaseScope labeling of SV2A, SV2B, and SV2C transcripts as well as for the detection of SV2Aexon3, we strictly followed the instructions provided by ACD Biotechne. Briefly, PFA-fixed frozen brain sections were prepared with antigen retrieval treatment, followed by hydrogen peroxide, RNA target retrieval, and protease incubation. For RNAscope and BaseScope assays, SV2A, SV2B, and SV2C probes (RNAscope) and SV2Aexon3 (BaseScope) were hybridized for 2 h, before multiple sequential signal amplification steps. For the codetection of RNA and proteins, these protocols were followed by immunofluorescent stainings, as described above. Images were acquired with an FV1000 (Olympus) or Nikon A1R (Nikon) confocal microscope.

Exploration of single-cell RNAseq datasets

In order to support our RNAscope results with quantitative data, we investigated publicly available single-cell RNA sequencing data using the Single Cell Portal online tool (https://singlecell.broadinstitute.org/single_cell). We interrogated the expression of SV2A, SV2B, and SV2C in two datasets that include gene expression data from different cell types from the adult mouse hippocampus (Habib et al., 2016; Russell et al., 2023).

Elecroencephalogram (EEG) electrode implantation

Mice (six PV:SV2A-cKO vs five WT littermates, and three SST:SV2A-cKO vs three WT littermates) were anesthetized with isoflurane (5% for induction, 2% for maintenance) and fixed in the stereotactic frame. A midline incision is made in the skin above the skull, and sutures (bregma/lambda) are visualized. One burr hole (1 mm diameter) was made for the placement of an epidural ground electrode. This electrode was custom-made and consisted of a microscrew (1 mm diameter, Fabory) soldered to an insulated copper wire. At the connector side, the wire was soldered to a Winslow connector pin (267–7400, RS components). Another burr hole is made above the right hippocampus (coordinates, −2.0 mm AP and +1.8 mm ML relative to bregma) for implantation of a bipolar depth recording electrode (200 µm tip separation, custom-made by twisting two stainless steel wires, California fine wire, 70 µm bare diameter). At the connector side, electrode wires are sandwiched between two Winslow connector pins. The recording electrode tip was positioned in the brain 2 mm below the dura. Next, the Winslow connectors were assembled as a connector block and fixed to the skull with acrylic cement to make a head cap. During surgery, body temperature was maintained at 37°C by a thermoregulated heating pad. Postsurgery animals were treated with meloxicam (1 mg/kg) to manage pain.

EEG recordings

One week after implantation surgery, mice were connected to the EEG setup for recording (10 A.M.–6 P.M.). This setup consists of a head stage with a unity gain preamplifier (custom-made) connected to a six-channel cable and a commutator (SL6C six-channel commutator, Plastics One), allowing the animals to move freely. EEG signals were high-pass filtered at 0.15 Hz and amplified 512× (custom-made). An analog–digital convertor (NIDAQ card, National Instruments, USB-6259) was used to digitize EEG at a sampling rate of 2 kHz (16-bit resolution, ±10 V input range), and the output was stored on a PC for offline analysis. The

EEG traces were plotted (Matlab, MathWorks) and visually evaluated for epileptic activity. Electrographic seizures were defined as a repetitive pattern of complex, high-amplitude EEG spikes lasting at least 7 s at hippocampal electrodes. Consecutive seizures are separated by at least 7 s; otherwise, they are counted as one. An epileptiform spike is defined as a high amplitude, sharp (<70 ms) single or multiform spike on the EEG statistical analysis.

Experimental design and statistical analyses

Experiments were performed with >3 individuals per group and systematically compared cKO mice with their WT littermates. Statistical tests and graphics were realized with GraphPad Prism V8. Mann–Whitney test was used for all experiments comparing two groups. The level of statistical significance was set at $p < 0.05$. Results are displayed as median ± range. The number of animals (biological replicates) used in each experiment is indicated as *N* in the figure legends.

Results

The ubiquitous disruption of SV2A function during adulthood induces seizure

We previously described the first SV2A lox/lox mouse as a valuable basis to study the effect of a conditional SV2A knock-out (SV2A-cKO), and we showed that the recombination of SV2A at the level of a whole organism recapitulated the phenotype of the SV2A full KO mouse (Menten-Dedoyart et al., 2016). In this study, we harness the SV2A lox/lox mouse to unravel the function of SV2A in different cell types and at different brain development steps.

Inducible ubiquitin C (Ubc)-cre^{ERT2} mice were used to evaluate the effect of ubiquitous SV2A-cKO at adult age, after complete brain development. From postnatal day 60 (P60), mice were treated with tamoxifen for 5 consecutive days to induce functional *SV2A*-cKO, and their phenotype was observed since induction. Wild-type (WT) littermates receiving tamoxifen were used as controls. One to 2 months later, all Ubc:SV2A-cKO mice presented severe convulsive seizures, quickly followed by death (Fig. 1*A*), while WT mice displayed normal behavior and life expectancy. Western blot analysis confirmed a strongly reduced SV2A expression in the brain of Ubc:SV2A-cKO mice compared with WT (Fig. 1*B*). No modified expression of SV2B or SV2C was observed (Fig. 1*C*,*D*), indicating that SV2A deficiency is not compensated by SV2 isoforms. Consistent with earlier evidence showing lethal "status epilepticus" in SV2A full KO mice, these data show that the ubiquitous

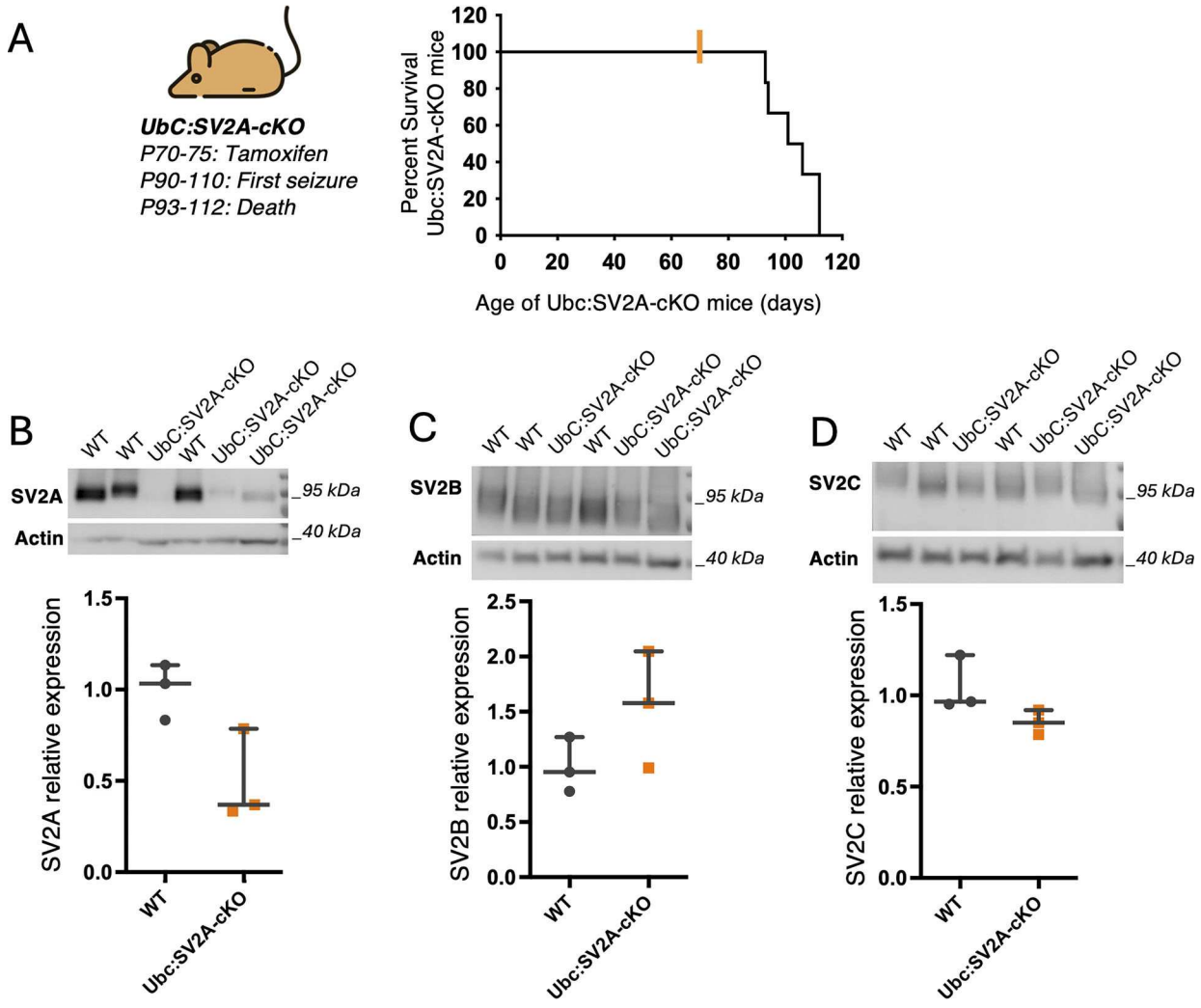

Figure 1. SV2A knock-out in adult UbC:Cre mice induces seizure. ***A***, Phenotype summary and survival of Ubc:SV2A-cKO mice after tamoxifen injection at P70 ($N = 6$ mice). ***B***, Western blot analysis of SV2A protein in Ubc:SV2A-cKO mice brain lysates (harvested after the first seizures were observed), normalized to the expression in WT brains ($p = 0.10$; $N = 3$ mice per group). ***C***, ***D***, Western blot analysis of SV2B and SV2C proteins in Ubc:SV2A-cKO brain lysates, normalized to the expression in WT brains (SV2B, $p = 0.20$; SV2C, $p = 0.10$; $N = 3$ mice per group). Statistics: Unpaired Mann–Whitney test, two-tailed with 95% confidence level. Data are represented as median with range.

knock-out of SV2A after development also leads to seizures when induced at the adult age.

Seizure is induced by SV2A functional KO in inhibitory neurons, but not in excitatory neurons

To identify which neuronal subtype SV2A defect results in seizures, we systematically narrowed down the neuron population targeted by SV2A recombination by using a panel of Cre mouse lines. First, we assessed the phenotype of Nestin:SV2A-cKO mice (Nes:SV2A-cKO), which shows recombination from E11, affecting all neurons (Tronche et al., 1999; Fig. 2*A*). Nes:SV2A-cKO mice exhibit clinical seizures around P12 and die 3–5 d later. Mice show a significantly reduced body weight at P12 (Fig. 2*B*). A Western blot analysis shows a significant reduction of SV2A (Fig. 2*C*) whereas the expression of SV2B or SV2C was not significantly modified (Fig. 2*D,E*). The brain morphology, cortical thickness, and neuronal density of Nes:SV2A-cKO mice are indistinguishable from WT (Fig. 2*F*). This phenotype recapitulates those of previous whole-animal SV2A-KO, validating the Cre-lox approach.

The next step was to compare the effects of SV2A deficiency in the two main types of excitable cells: glutamatergic and GABAergic neurons. Nex-cre mice were used to target telencephalic excitatory neurons (mainly pyramidal neurons; Goebbels et al., 2006). Nex:SV2A-cKO mice do not display seizures, have a normal life expectancy, and reproduce normally (Fig. 2*G*). Again, evaluation at the protein level shows that SV2A is correctly recombined in the brain (Fig. 2*H*) while SV2B and SV2C levels remain stable (Fig. 2*I,J*). The cortical thickness is similar for both the WT and Nex:SV2A-cKO mice (Fig. 2*K*). Accordingly, the density of neurons in upper and lower cortical layers, respectively, identified by CUX1 and CTIP2 labeling, indicates an unchanged number of cortical glutamatergic neurons.

Dlx-Cre mice were used to induce recombination in most GABAergic interneurons (Ruest et al., 2003). In contrast to what was observed for Nex:SV2A-cKO mice, Dlx:SV2A-cKO mice develop seizure around P15 and die 3–6 d later (Fig. 3*A*). At P16, the Dlx:SV2A-cKO mice have a significantly lower body weight compared with their WT counterparts (Fig. 3*B*). In this case, no significant reduction of SV2A protein was observed in brain lysates (data not shown), which can be attributed to the low proportion of interneurons in the whole brain. We verified using qPCR that *SV2A* mRNA level tends to be reduced in Dlx:SV2A-cKO mice brains compared with WT (Fig. 3*C*), and no change is observed for *SV2B* (Fig. 3*D*) and *SV2C* (Fig. 3*D*). Dlx:SV2A-cKO mice do not present any modified brain morphology, neuronal density, or cortical thickness, consistent with the absence of changes in pan-neuronal knockouts.

Next, we assessed the cortical and hippocampal neuron density of the two main populations of GABAergic interneurons using antibodies directed against parvalbumin (PV) and somatostatin (SST) proteins in Dlx:SV2A-cKO mice. The density of PV^+ and SST^+ neurons was quantified in the neocortex (more precisely in the somatosensory area, the posterior parietal area, and the primary visual area) and in the hippocampus (Fig. 3*F–I*). No change was observed in the cortex. In contrast, the density of PV^+ interneurons in the hippocampus was significantly reduced in Dlx:SV2A-cKO at P16, corresponding to the first seizure experience, compared with WT (Fig. 3*H*). The defect seems to be spread across the whole hippocampus as no significant differences were found between the "dentate gyrus," CA1, and CA3. In the hippocampus, no change in SST^+ neurons was noticed.

Proteomic analysis reveals minor changes in SV2A-deficient synaptosomes derived from glutamatergic neurons and interneurons

We decided to search for new proteins that could interact with SV2A or could be differentially expressed upon SV2A-cKO, by investigating the synaptic compartment of SV2A-deficient neurons. We first showed that isolated synaptosome fractions are enriched in classical synaptic proteins, e.g., PSD95 (Fig. 4*A,B*). We also showed that SV2A is present, with apparent reduction in Nex:SV2A-cKO synaptosome fractions (Fig. 4*C*). We then compared the whole protein content of synaptosomes using mass spectrometry. Synaptosomes were isolated at P20 from the hippocampi of Dlx:SV2A-cKO, Nex:SV2A-cKO and WT mice (four hippocampal synaptosome extracts per group). A list of 4,297 proteins were identified in all groups. Among these, only 172 proteins (4%) were significantly affected by SV2A-cKO (Tukey test post-ANOVA, $p < 0.05$; Fig. 4*D*). SV2A was detected and a statistically significant reduction was observed in Nex:SV2A-cKO, in concordance with our previous results (Fig. 4*E*). SV2B was detected as consistently abundant in all groups (Fig. 4*F*), as well as Syt1 (Fig. 4*G*). Other typical synaptic proteins were also detected, e.g., Snap25, synaptophysin, and syntaxin, but not differentially abundant in SV2A:cKO animals (Extended Data Table 2-1). Only 13 proteins were found differentially abundant in Nex:SV2A-cKO synaptosomes specifically, compared with WT, despite SV2A invalidation in most neurons of the extract. In Dlx:SV2A-cKO synaptosomes, only 15 proteins were found differentially abundant compared with WT, despite the important seizure phenotype observed in these mice (Fig. 4*H,I*). Finally, 31 proteins were commonly modified in Nex:SV2A-cKO and Dlx:SV2A-cKO synaptosomes, compared with WT (Fig. 4*J*). Taken together, these results reveal that only a few proteins appear influenced by SV2A-cKO, over the few thousands of proteins detected. This may indicate that the mechanisms that are responsible for seizure onset upon Dlx:SV2A-cKO exclusively may not be linked to a significant modulation of the synaptic proteome.

Selective SV2A:cKO in parvalbumin interneurons leads to early onset seizure

Established that GABAergic neurons require SV2A for regular neurotransmission, we aimed to provide a way to determine whether one subtype of inhibitory neurons could be responsible for the epileptic phenotype upon SV2A-cKO. As the GABAergic neuron population includes several interneuron subtypes that can be distinguished by different molecular markers, we used three mouse lines targeting the three main subpopulations of GABAergic interneurons (PV:cre, SST:cre, and VIP:cre) and crossed them with the SV2A lox/lox mouse to induce SV2A recombination specifically in those neuronal subtypes. Interestingly, PV:SV2A-cKO mice show clinical seizures around P16–P20, associated with a reduced lifespan of 21–50 d (Fig. 5*A,B*). Compared to the other mouse lines with seizure (i.e., Nes:SV2A-cKO or Dlx:SV2A-cKO), a significant reduction of body weight in PV:SV2A-cKO is only observed from P27 (Fig. 5*C*). Given the low proportion of PV neurons across the cortex or the hippocampus, we could not consider protein or mRNA analyses on whole tissue lysates to properly validate SV2A-cKO. We used BaseScope to validate the recombination in PV:SV2A-cKO mice, using a probe targeting the third exon of the SV2A gene. No *SV2A* mRNA was detected in PV neurons from PV:SV2A-cKO tissue, in contrast to WT (Fig. 5*D*), thereby validating the correct recombination of the SV2A gene in PV

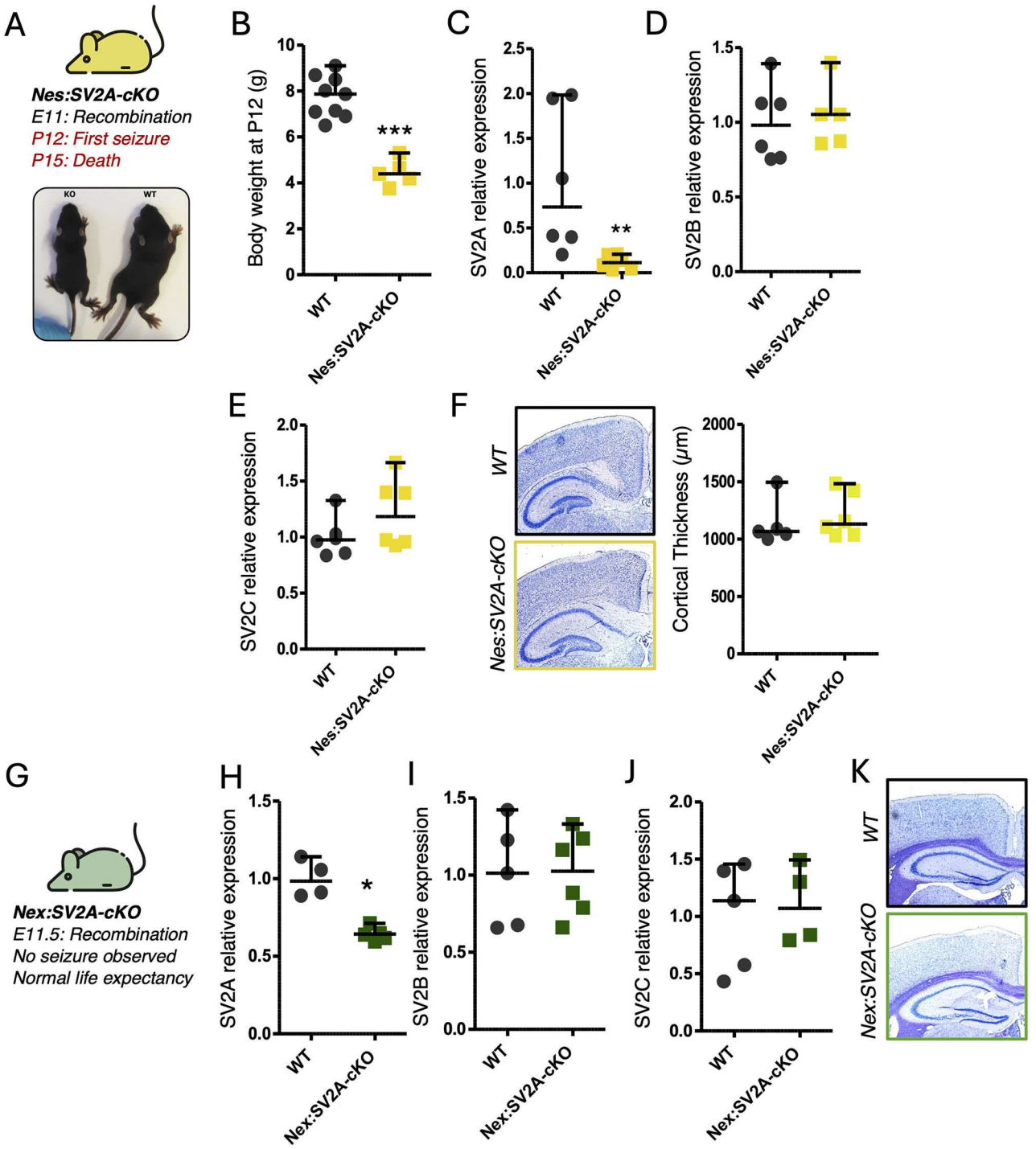

Figure 2. SV2A knock-out in all neural cells induces seizure but does not elicit a specific phenotype when occurring only in glutamatergic neurons. ***A***, Phenotype summary for Nes:SV2A-cKO mice. ***B***, Body weight measurement in Nes:SV2A-cKO compared with WT mice, at P12 ($p = 0.001$; $N = 5$ and $N = 9$ mice per group). ***C***, Western blot analysis of SV2A protein in Nes:SV2A-cKO mice (whole-brain lysates), compared with WT ($p = 0.0043$; $N = 6$ mice per group) ***D***, ***E***. Quantification of Western blot signals observed for SV2B and SV2C expression in Nes:SV2A-cKO whole-brain lysates compared with WT brains (SV2B, $p = 0.6623$; SV2C, $p = 0.3095$; $N = 5$–6 mice per group). ***F***. Representative toluidine blue stainings and quantification of the cortical thickness of Nes:SV2A-cKO mice at P12 ($p = 0.6623$; $N = 5$–6 mice per group). ***G***, Phenotype summary for Nex:SV2A-cKO mice. ***H***, Western blot analysis of SV2A protein in Nex:SV2A-cKO mice (whole-brain lysates), compared with WT ($p = 0.0159$; $N = 4$–5 mice per group). ***I***, ***J***, Quantification of Western blot signals observed for SV2B and SV2C expression in Nex:SV2A-cKO whole-brain lysates compared with WT (SV2B, $p = 0.9307$; SV2C, $p = 0.7302$; $N = 4$–6 mice per group). ***K***, Representative toluidine blue stainings of the cortex and hippocampus of Nex:SV2A-cKO mice compared with WT (see quantification on Extended Data Fig. 1-1). Statistics: Unpaired Mann–Whitney test, two-tailed with 95% confidence level. Data are represented as median with range.

neurons. It therefore appears that the loss of SV2A in PV neurons alone would account for most of the seizure phenotype observed in SV2A total KO. We quantified PV^+ and SST^+ neuron density in the cortex and the hippocampus of PV:SV2A-cKO and WT mice. No significant difference could be observed at P16 in PV:SV2A-cKO (Fig. 5*E–H*). However, we observed a significant increase in apoptotic, caspase-3–positive cells in the hippocampus of PV:SV2A-cKO mice (Fig. 5*I*) that corresponded to excitatory neurons, inhibitory neurons, and microglial cells. To get more insight into the functional consequences of the SV2A:cKO in PV

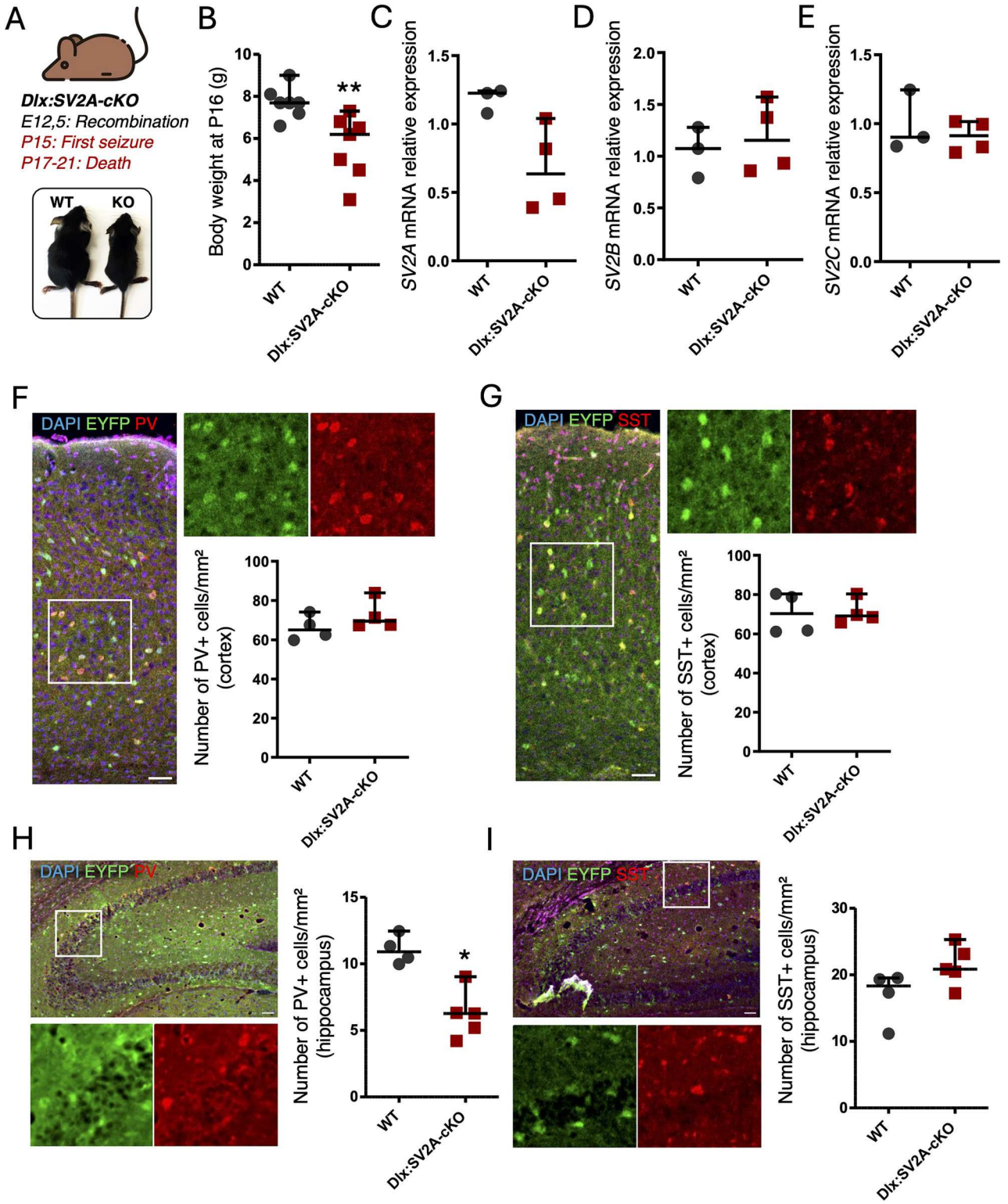

Figure 3. SV2A knock-out in inhibitory neurons induces seizure. ***A***, Summary of Dlx:SV2A-cKO mouse phenotype. ***B***, Body weight measurement in Dlx:SV2A-cKO compared with WT mice, at P12 ($p = 0.007$; $N = 7$ mice per group). ***C***, qRT-PCR analysis of *SV2A* mRNA in Dlx:SV2A-cKO brain cDNA samples, compared with WT brain samples ($p = 0.057$; $N = 3$–4 mice per group). ***D***, ***E***, qRT-PCR analysis of *SV2B* and *SV2C* mRNA in Dlx:SV2A-cKO brain cDNA samples, compared with WT brain samples (SV2B, $p = 0.6286$; SV2C, $p = 0.6286$; $N = 3$–4 mice per group). ***F***, Immunofluorescent costaining of EYFP (green, showing Dlx:Cre recombined cells) and PV (red) and calculated density of cortical PV^+ neurons at P16 ($p = 0.6286$; $N = 4$ mice per group). ***G***, Immunofluorescent costaining of EYFP (green, showing Dlx:Cre recombined cells) and SST (red) and calculated density of cortical SST^+ neurons at P16 ($p = 0.8571$; $N = 4$ mice per group). ***H***, Immunofluorescent costaining of EYFP (green, showing Dlx:Cre recombined cells) and PV (red) and calculated density of hippocampal PV^+ neurons at P16 ($p = 0.0159$; $N = 4$–5 mice per group). ***I***, Immunofluorescent costaining of EYFP (green, showing Dlx:Cre recombined cells) and SST (red) and calculated density of hippocampal SST^+ neurons at P16 ($p = 0.1111$; $N = 4$–5 mice per group). Statistics: Unpaired Mann–Whitney test, two-tailed with 95% confidence level. Data are represented as median with range. Scale bar, 50 µm.

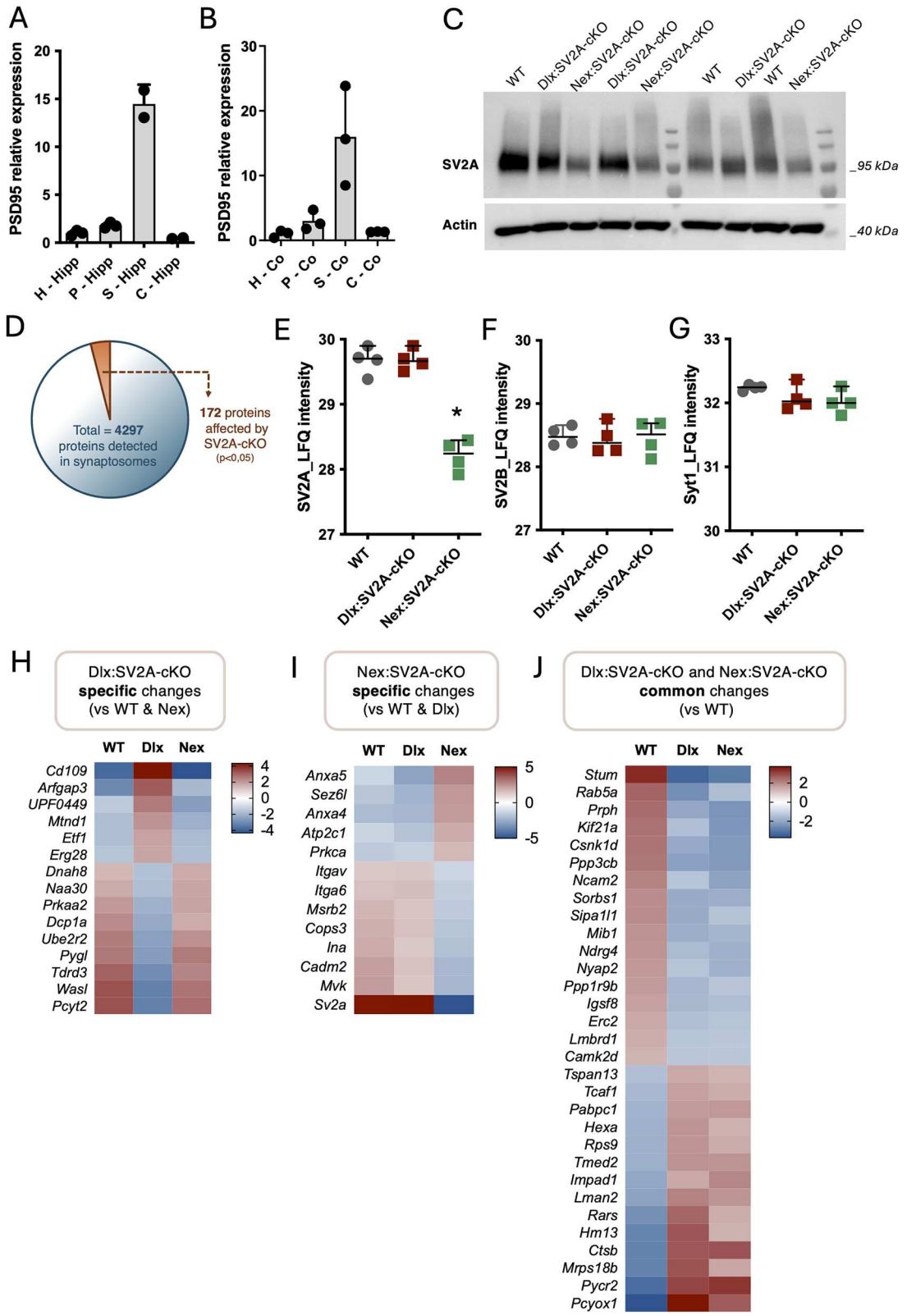

Figure 4. Mass spectrometry identifies various changes in protein abundance in isolated Dlx:SV2A-cKO and Nex:SV2A-cKO brain synaptosomes, compared with WT synaptosomes. ***A***, ***B***, Expression of PSD95 in total homogenate (H), pellet (P), synaptosomal fraction (S), and supernatant (*C*), using hippocampal lysates (Hipp) and cortex lysates (Co; $N = 2–3$ mice per group). ***C***, Western blot analysis of SV2A expression in Dlx:SV2A-cKO, Nex:SV2A-cKO, and WT synaptosomes ($N = 3$ mice per group). ***D***, Pie chart representing the 4,297 proteins identified in at least one synaptosomal fraction, with only 172 proteins significantly impacted by SV2A-cKO. ***E***, LFQ intensity data on SV2A abundance in Dlx:SV2A-cKO, Nex:SV2A-cKO, and WT synaptosomes ($p = 0.0145$; $N = 4$ mice per group). ***F***, ***G***, LFQ intensity data on SV2B and Syt1 abundance in Dlx:SV2A-cKO, Nex:SV2A-cKO and WT synaptosomes (SV2B, $p = 0.0676$; Syt1, $p = 0.3271$; $N = 4$ mice per group). Statistic test: Unpaired Mann–Whitney test, two-tailed with 95% confidence level. Data are represented as median with range. ***G***, Venn diagram representing the 59 proteins that show a statistically significant differential abundance across groups, in synaptosomal fractions. Statistic test: ANOVA, two-tailed with 95% confidence level, followed by Tukey's test. ***H–J***, Heatmap of the differentially abundant synaptic proteins specifically impacted by SV2A recombination in Dlx:SV2A-cKO synaptosomes (***H***), Nex = SV2A-cKO synaptosomes (***I***), and WT synaptosomes (***J***). Data are represented as the log *p*-value of the ANOVA analysis. Positive values represent an increase in protein abundance, and negative values represent a decrease in protein abundance.

neurons, we performed EEG recordings at P20 and detected abnormal electrical activities in all recorded PV:SV2A-cKO mice, but not in WT mice. Several types of seizure activity were observed, as well as epileptic spikes (Fig. 5*J,K*).

We also investigated SST:SV2A-cKO mice (Fig. 6*A*), in which we validated the proper deletion of SV2A using BaseScope (Fig. 6*B*). Over the multiple generations of mice that have been observed, only one SST:SV2A-cKO mice displayed a clinically observable seizure around P71, followed by death at P82. We therefore performed EEG recordings on adult SST:SV2A-cKO mice, to further evaluate epileptic activities. Three SST:SV2A-cKO mice were analyzed, and all of them presented epileptic spikes. Two out of these three animals displayed epileptic seizures followed by death at P98 and P104 (Fig. 6*C,D*).

Finally, no phenotype was observed in VIP:SV2A-cKO mice: they appear normal, reproduce well, and survive normally, and no seizure was ever observed; hence, no further analysis was carried out.

SV2 isoforms are differentially distributed in the hippocampus

Our results have shown that the SV2A invalidation in UbC:SV2A-cKO, Nes:SV2A-cKO, and Dlx:SV2A-cKO leads to seizure and that the loss of SV2A is not compensated by any upregulation of SV2B and SV2C. Taking advantage of the RNAscope technology, we aimed at a qualitative evaluation of the distribution of these three SV2 isoforms in the hippocampus, to shed light on the neuronal populations that express either of them. We observed that SV2A is expressed not only in pyramidal cells but also in interneurons across the CA1 and CA3 and in the dentate gyrus (DG; Fig. 7*A,B*). In contrast, SV2B seems restricted to pyramidal neurons, especially in the CA3 region (Fig. 7*A*). SV2C is highly expressed not only in granule cells from the DG but also in interneurons (Fig. 7*B*). These results are in line with previous gene expression data in the rat brain and human cortex that also showed that *SV2A* is expressed in all types of neurons, whereas *SV2B* seems restricted to excitatory neurons and *SV2C* further limited to a subset of cortical interneurons (Pazarlar et al., 2022). This differential distribution of SV2 s is also strongly supported by recent single-cell RNAseq data that show a similar expression pattern for *SV2* isoforms in diverse hippocampal neuron types from the adult mouse brain (Fig. 7*C,D*). Note that a similar distribution of SV2 s was observed in PV:SV2A-cKO animals, further supporting the idea that the seizure phenotype upon SV2A invalidation is likely not associated with a compensation from other SV2 isoforms.

Discussion

The synaptic vesicle glycoprotein 2A has long been associated with epilepsy, based on the seizure phenotype observed in SV2A-KO mice (Crowder et al., 1999; Janz et al., 1999) and the reduced SV2A expression observed in resected human epileptic tissue (Toering et al., 2009; Van Vliet et al., 2009). SV2A expression has been shown to be a prerequisite for levetiracetam therapeutic activity of levetiracetam in mouse models (Lynch et al., 2004), and mutations in *SV2A (*Serajee and Huq, 2015; Wang et al., 2019; Calame et al., 2021*)* have so far been identified in epileptic patients and associated to an altered response to levetiracetam.

In this study, we confirmed that the ubiquitous SV2A-cKO at adult age triggers a lethal seizure, and we identified parvalbumin (PV) interneurons as the neuronal population in which SV2A defects induce a lethal epileptic seizure in the premature brain. These findings are consistent with the interpretation that PV neurons play an outsized role in seizure development. They also suggest that levetiracetam's antiseizure action may be due primarily to an effect on PV neuron activity.

PV neurons are known to be associated with epilepsy, as a decrease in PV neuron density was reported in human tissue from resected epileptic foci (Zamecnik et al., 2006; Andrioli et al., 2007; Nakagawa et al., 2017). Other studies showed that while PV neuronal bodies and synapse numbers remain stable in epileptic tissues, the ratio of functional PV neuron subsets (i.e., basket cells vs chandelier cells) was modified (Alhourani et al., 2020). Consistent findings were raised in different studies using animal models of epilepsy. A significant loss of PV neurons was observed in TLE models, e.g., a kainate mouse model (Marx et al., 2013), and in a sea lion model exposed to domoic acid (Cameron et al., 2019). In a rat model of injury-induced epilepsy, cortical PV neuron density is preserved, but their morphology, synaptic content, and firing pattern were reported to be affected (Gu et al., 2017). Although these observations converge on the key role that PV neurons play in epileptic disease, they hardly inform us about whether PV neuron loss is a cause or a consequence. In contrast, the findings reported here show that SV2A deficiency in PV neurons can induce a seizure phenotype, consistent with the interpretation that aberrant PV neuron function can induce seizures. In a PTZ model combined with optogenetic regulation of interneuron activity and electrophysiology, it has been shown that granule cell inhibition by PV and SST neurons remains intact during the preictal and early ictal phases. However, PV and SST interneurons show specific differences in their preictal firing pattern and sensitivity to neuronal input. This suggests that an altered interneuron network activity precedes seizure onset, within the hippocampal circuit (Miri et al., 2018).

Whereas seizure onset is observed at postnatal day 7 (P7) in the SV2A full KO model (Crowder et al., 1999; Janz et al., 1999), our study describes seizure onset around P15 upon SV2A invalidation in all GABAergic neurons (Dlx:SV2A-cKO mice) or at P16–21 when only PV neurons are concerned by the defect (PV:SV2A-cKO). Finally, several SST:SV2A-cKO mice developed seizure later around P80–100. We observed a decrease in PV^+ neuron number in the Dlx:SV2A-cKO mice at P15, but no difference in the PV:SV2A-cKO mice, despite a similar seizure phenotype. This could be explained by the larger number of neurons affected by SV2A deficiency and subsequent seizure, which may result in a higher degree of cell death in the Dlx:SV2A-cKO model. Note that the initiation of SV2A recombination and the targeted subtypes of neurons are different in those two models, warranting cautious conclusions and fostering further experiments. Of note, no apparent gender difference was observed in any of the mouse lines.

These results also suggest that hippocampal PV neurons are particularly affected by SV2A invalidation, as cortical PV neuron number appears unaffected in the Dlx:SV2A-cKO mice. The hippocampus has a high neuronal and synaptic density (Keller et al., 2018; Santuy et al., 2020), while presenting an average number of PV neurons (Bjerke et al., 2021). This may suggest that the hippocampus is more vulnerable to PV neuron deficiency. Finally, as parvalbumin is an activity-dependent gene (Favuzzi et al., 2017; Shi et al., 2019), we can't rule out the possibility that the reduced PV cell density may hide a reduced activity of PV neurons.

The proteomic comparison of synaptosomal fractions revealed only a few differentially abundant synaptic proteins

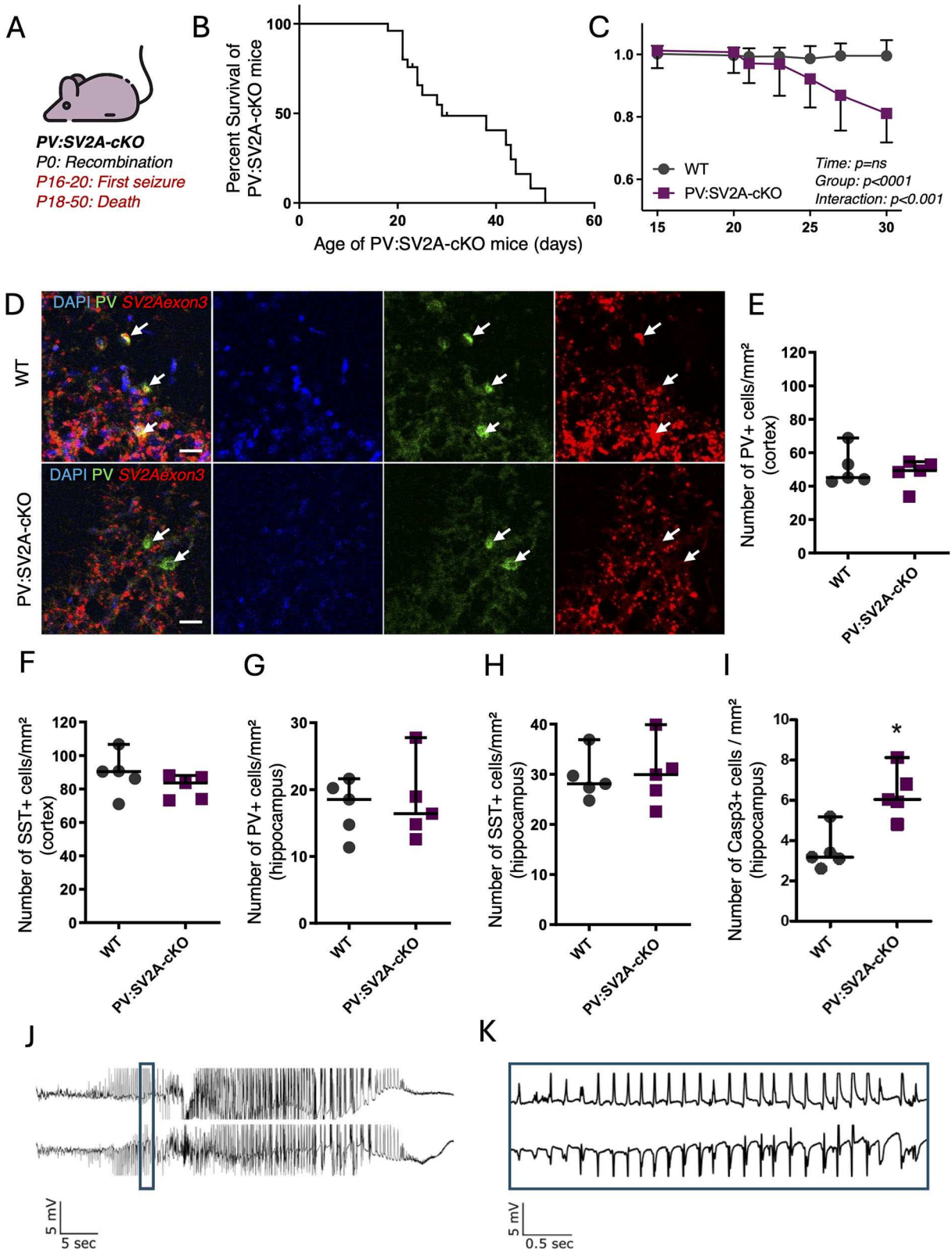

Figure 5. SV2A knock-out in parvalbumin interneurons leads to lethal seizure. ***A***, Summary of PV:SV2A-cKO mouse phenotype. ***B***, Survival curve of PV:SV2A-cKO mice ($N = 25$ mice). ***C***, Evolution of body weight in PV:SV2A-cKO and WT mice from P15 to P30 (P2). Statistic test: two-way ANOVA ("time" vs "group") with Bonferroni's post hoc test, 95% confidence level. ***D***, BaseScope colabeling of PV (green) and the third exon of SV2A (red) in the hippocampus CA3 region of WT or PV:SV2A-cKO. Arrowheads highlight PV^+ neurons. Scale bar, 40 µm. ***E***, Density of cortical PV^+ neurons at P16 ($p = 1$; $N = 5$ mice per group). ***F***, Density of cortical SST^+ neurons at P16 ($p = 0.3095$; $N = 5$ mice per group). ***G***, Density of hippocampal PV^+ neurons at P16 ($p = 1$; $N = 5$ mice per group). ***H***, Density of hippocampal SST^+ neurons at P16 ($p = 0.8413$; $N = 5$ mice per group). ***I***, Density of hippocampal caspase-3–positive cells at P16 ($p = 0.0159$; $N = 5$ mice per group). Statistic test: Unpaired Mann–Whitney test, two-tailed with 95% confidence level. Data are represented as median with range. ***J***, Representative EEG traces recorded in PV:SV2A-cKO mice during seizures. ***K***, Close-up of epileptiform discharges.

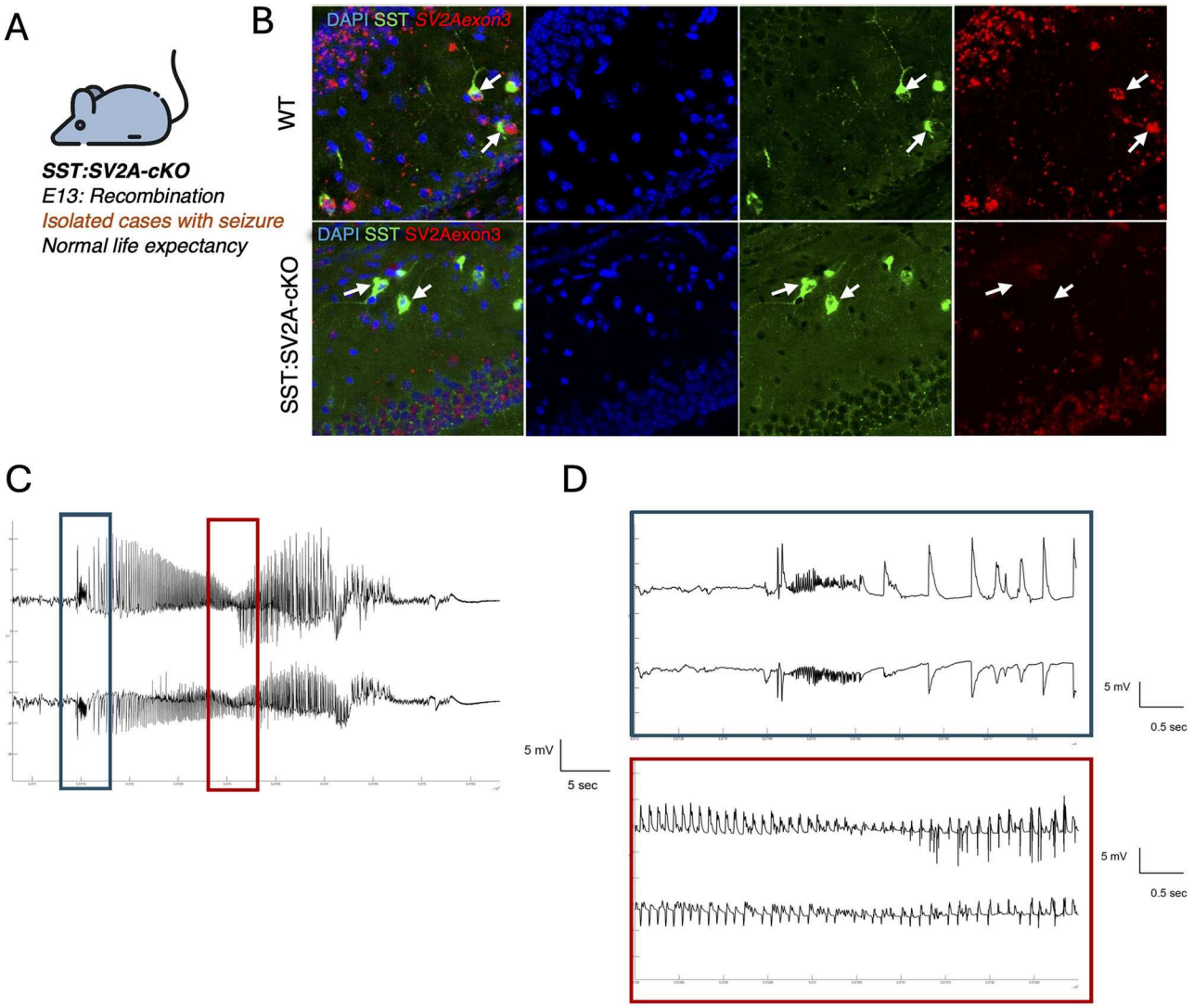

Figure 6. SV2A knock-out in somatostatin interneurons triggers epileptic discharges. ***A***, Summary of SST:SV2A-cKO mouse phenotype. ***B***, BaseScope colabeling of SST (green) and the third exon of SV2A (red) in the hippocampus CA1 region of WT or PV:SV2A-cKO. Arrowheads highlight SST^+ neurons. Scale bar, 40 µm. ***C***, Example of EEG traces recorder in one SST:SV2A-cKO mouse.

upon SV2A-cKO, especially when comparing Dlx:SV2A-cKO mice (with seizure) compared with WT and Nex:SV2A-cKO mice (without seizure). We therefore hypothesize that the functional consequences of SV2A invalidation may not be associated with massive variations in the synaptic protein content but rather could be related to the functional effects on the individual cell types. To us, this would especially make sense for PV interneurons. First, PV neurons are known for their acute and high need for ATP, high energetic machinery, and mitochondrial volume compared with other inhibitory neurons (Kageyama and Wong-Riley, 1982; Gulyás et al., 2006; Adams et al., 2015; Takács et al., 2015; Paul et al., 2017). The absence of SV2A has been shown to increase the speed of SV recycling (Kaempf et al., 2015; Bae et al., 2020), a process that is highly ATP-consuming (Heidelberger, 2001; Kann et al., 2014; Egashira et al., 2015; Pathak et al., 2015). Increased SV recycling upon loss of SV2A could therefore induce energy failure in these neurons. Another hypothesis emerges from the fact that PV neurons express many different synaptotagmin paralogs (i.e., Syt2, 4, 5, 7, 12, and 13; Bartholome et al., 2020). Whereas SV2A is known to interact with Syt1, it would be interesting to explore SV2A interaction with these other isoforms, especially if some of them are PV-specific. For instance, Syt2 has been suggested as a potential marker for PV neurons in the visual cortex (Sommeijer and Levelt, 2012). Finally, PV neurons are also known to establish perineuronal nets (PNN), a specialized extracellular matrix structure mainly formed by proteoglycans (Bartholome et al., 2020). Interestingly, PNNs settle around P10 and are known to influence synaptic function and plasticity. SV2A is itself a keratan sulfate integral membrane proteoglycan (Scranton et al., 1993), with multiple *N*-glycosylation sites placed toward the extracellular compartment; hence, a potential interaction of SV2A with those PNNs could be considered.

Elucidating the phenotype of SST:SV2A-cKO mice based on our results is trickier. The large majority of SST:SV2A-cKO animals were able to reproduce and live for more than a year. Still, we observed one SST:SV2A-cKO mouse with spontaneous seizures at several months of age, which died shortly after. EEG recordings on three other individuals showed altered neuronal activity and subsequent death. STT neurons have also been associated with epilepsy in other studies. For example, an increased SST axonal sprouting has been reported in different animal

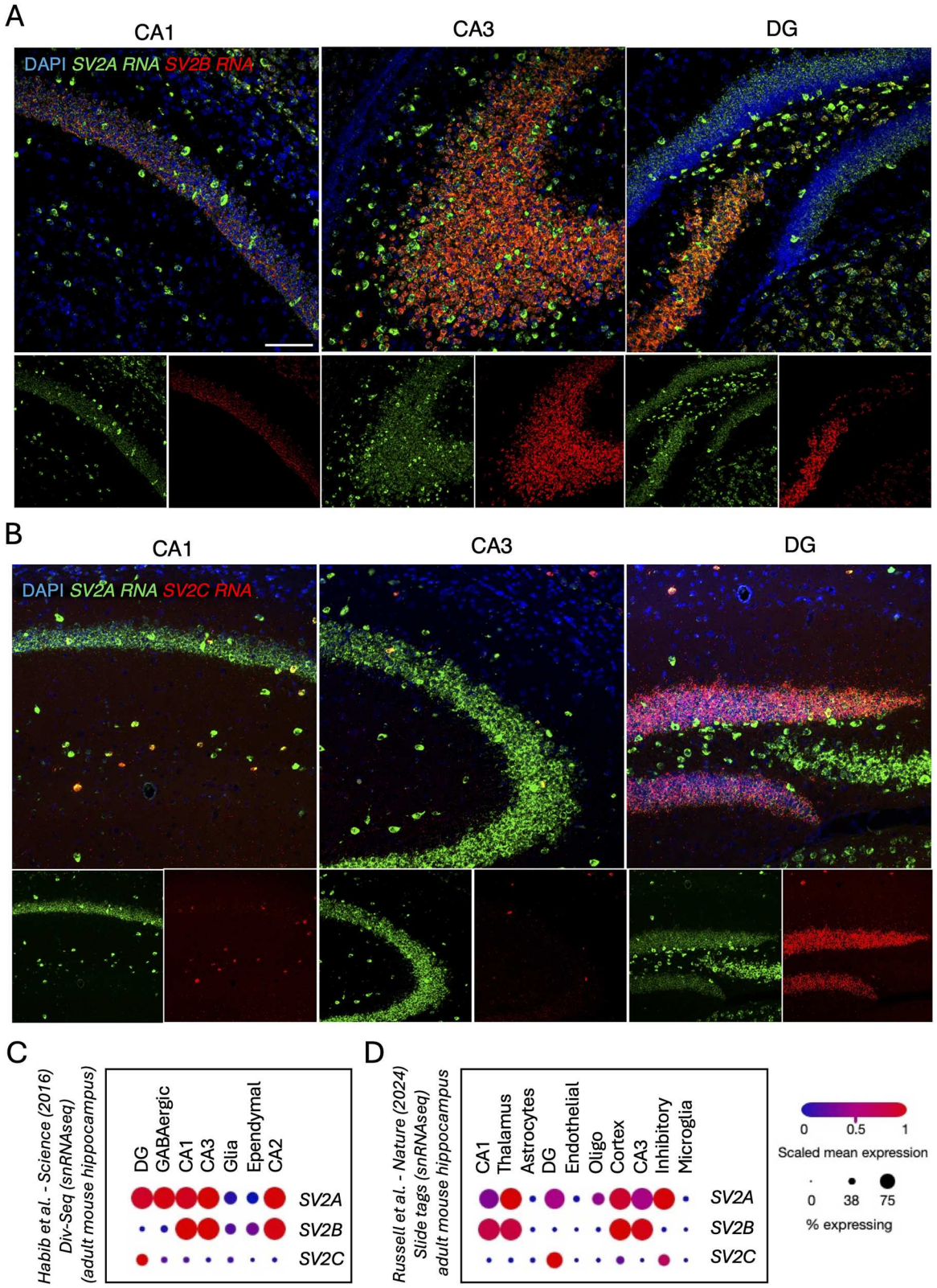

Figure 7. SV2 isoforms show differential expression in the adult mouse hippocampus. ***A***, RNAscope colabeling of *SV2A* and *SV2B* mRNA in the CA1, CA3, and DG regions of the adult mouse hippocampus. ***B***, RNAscope colabeling of *SV2A* and *SV2C* mRNA in the CA1, CA3, and DG regions of the adult mouse hippocampus. Scale bar, 100 µm. ***C***, ***D***, Expression of SV2 isoforms in different neuron populations from the adult mouse hippocampus. Data extracted from Single Cell Portal (Broad Institute).

models of epilepsy (Zhang et al., 2009; Buckmaster and Wen, 2011), and SST neuronal activity is reduced in the neocortex of a murine model of Dravet syndrome (Tai et al., 2014). A recent large-scale analysis of more than 110.000 neuronal transcriptomes from patients suffering from temporal lobe epilepsy versus controls revealed that both PV and SST interneurons contain

more changes than other inhibitory neuron subtypes (Pfisterer et al., 2020). To our knowledge, SST neurons do not have a particularly high energy demand, contrary to PV cells, which could explain why they appear differently affected by SV2A-cKO (Gulyás et al., 2006; Paul et al., 2017). It is also plausible that SV2A deficiency would induce a similar cascade of events in PV and SST neurons that would happen at a different pace, leading to a variable seizure onset. The genuine determinants of the particular PV neuron vulnerability to SV2A deficiency remain to be elucidated.

In contrast, the SV2A-cKO in Nex^{+} glutamatergic neurons (i.e., major subpopulation of neurons) did not recapitulate the epileptic phenotype that was observed when deleting SV2A in interneurons, putatively due to the presence of SV2B in these neurons. We note, however, that while the recombination of SV2A in CA3 pyramidal neurons using the Grik4-cre mouse line did not also elicit any observable seizure, it did produce an anxiety-like phenotype and spatial memory defects (Menten-Dedoyart et al., 2016; Serrano et al., 2019). However, no EEG recordings have been performed on any of those mice, and we cannot rule out the occurrence of subclinical seizure. On the other hand, glutamatergic neurons both express SV2A and SV2B (Bajjalieh et al., 1994; Pazarlar et al., 2022), which may suggest that the unique presence of SV2A or SV2B could protect from lethal seizures. Note that SV2B remains stable upon SV2A-cKO in glutamatergic neurons, and SV2B full KO animals do not display a lethal epileptic phenotype (Janz et al., 1999). However, in contrast to *SV2B*, we and others have observed that *SV2C* is expressed with SV2A in granule cells from the dentate gyrus and in interneurons (Habib et al., 2016; Russell et al., 2023) and is maintained in PV:SV2A-cKO interneurons in our experiments. These results rule out that SV2C would compensate for SV2A deficiency in the dentate gyrus.

Taken together, our results support the crucial part that SV2A plays in inhibitory neurons, clarifying the consequences of SV2A-cKO at the level of restricted neuronal populations and putatively at different stages of life, in relation to the epileptic phenotype. Of note, a functional assessment of synaptic function and neurotransmission defects leading to seizure is fundamental for a comprehensive elucidation of SV2A's role in epilepsy and warrants further investigation. As SV2A already is a key target in the pharmacological treatment of epilepsy, deciphering the mechanism of action of this synaptic protein might pave the way toward an improved patient care.

References

Adams DL, Economides JR, Horton JC (2015) Co-localization of glutamic acid decarboxylase and vesicular GABA transporter in cytochrome oxidase patches of macaque striate cortex. Vis Neurosci 32:10–13.

Alhourani A, et al. (2020) GABA bouton subpopulations in the human dentate gyrus are differentially altered in mesial temporal lobe epilepsy. J Neurophysiology 123:392–403.

Andrioli A, Alonso-Nanclares L, Arellano JI, DeFelipe J (2007) Quantitative analysis of parvalbumin-immunoreactive cells in the human epileptic hippocampus. Neuroscience 149:131–143.

Bae JR, et al. (2020) Distinct synaptic vesicle recycling in inhibitory nerve terminals is coordinated by SV2A. Prog Neurobiol 194:101879.

Bajjalieh SM, Frantz GD, Weimann JM, McConnell SK, Scheller RH (1994) Differential expression of synaptic vesicle protein 2 (SV2) isoforms. J Neurosci 14:5223–5235.

Bartholome O, de la Brassinne Bonardeaux O, Neirinckx V, Rogister B (2020) A composite sketch of fast-spiking parvalbumin-positive neurons. Cereb Cortex Commun 1:1–15.

Beghi E, et al. (2019) Global, regional, and national burden of epilepsy, 1990–2016: a systematic analysis for the global burden of disease study 2016. Lancet Neurol 18:357–375.

Bjerke IE, et al. (2021) Densities and numbers of calbindin and parvalbumin positive neurons across the rat and mouse brain. iScience 24:101906.

Buckmaster PS, Wen X (2011) Rapamycin suppresses axon sprouting by somatostatin interneurons in a mouse model of temporal lobe epilepsy. Epilepsia 52:2057–2064.

Calame DG, Herman I, Riviello JJ (2021) A de novo heterozygous rare variant in SV2A causes epilepsy and levetiracetam-induced drug-resistant status epilepticus. Epilepsy Behav Rep 15:100425.

Cameron S, et al. (2019) Proportional loss of parvalbumin-immunoreactive synaptic boutons and granule cells from the hippocampus of sea lions with temporal lobe epilepsy. J Comp Neurol 527:2341–2355.

Crowder KM, et al. (1999) Abnormal neurotransmission in mice lacking synaptic vesicle protein 2A (SV2A). Proc Natl Acad Sci U S A 96: 15268–15273.

Dossi E, Huberfeld G (2023) GABAergic circuits drive focal seizures. Neurobiol Dis 180:106102.

Egashira Y, Takase M, Takamori S (2015) Monitoring of vacuolar-type H+ ATPase-mediated proton influx into synaptic vesicles. J Neurosci 35:3701–3710.

Elahian B, et al. (2018) Low-voltage fast seizures in humans begin with increased interneuron firing. Ann Neurol 84:588–600.

Favuzzi E, et al. (2017) Activity-dependent gating of parvalbumin interneuron function by the perineuronal Net protein brevican. Neuron 95:639–655.e10.

Goebbels S, et al. (2006) Genetic targeting of principal neurons in neocortex and hippocampus of NEX-Cre mice. Genesis 44:611–621.

Grasse DW, Karunakaran S, Moxon KA (2013) Neuronal synchrony and the transition to spontaneous seizures. Exp Neurol 248:72–84.

Gu F, et al. (2017) Structural alterations in fast-spiking GABAergic interneurons in a model of posttraumatic neocortical epileptogenesis. Neurobiol Dis 108:100–114.

Gulyás AI, Buzsáki G, Freund TF, Hirase H (2006) Populations of hippocampal inhibitory neurons express different levels of cytochrome c. Eur J Neurosci 23:2581–2594.

Habib N, et al. (2016) Div-Seq: single-nucleus RNA-Seq reveals dynamics of rare adult newborn neurons. Science 353:925–928.

Heidelberger R (2001) ATP is required at an early step in compensatory endocytosis in synaptic terminals. J Neurosci 21:6467–6474.

Janz R, Goda Y, Geppert M, Missler M, Südhof TC (1999) SV2A and SV2B function as redundant Ca2+ regulators in neurotransmitter release. Neuron 24:1003–1016.

Kaempf N, et al. (2015) Overlapping functions of stonin 2 and SV2 in sorting of the calcium sensor synaptotagmin 1 to synaptic vesicles. Proc Natl Acad Sci U S A 112:7297–7302.

Kageyama GH, Wong-Riley MTT (1982) Histochemical localization of cytochrome oxidase in the hippocampus: correlation with specific neuronal types and afferent pathways. Neuroscience 7:2337–2361.

Kann O, Papageorgiou IE, Draguhn A (2014) Highly energized inhibitory interneurons are a central element for information processing in cortical networks. J Cereb Blood Flow Metab 34:1270–1282.

Keller D, Erö C, Markram H (2018) Cell densities in the mouse brain: a systematic review. Front Neuroanat 12.

Librizzi L, et al. (2017) Interneuronal network activity at the onset of seizure-like events in entorhinal cortex slices. J Neurosci 37:10398–10407.

Löscher W, Gillard M, Sands ZA, Kaminski RM, Klitgaard H (2016) Synaptic vesicle glycoprotein 2A ligands in the treatment of epilepsy and beyond. CNS Drugs 30:1055–1077.

Lynch BA, et al. (2004) The synaptic vesicle protein SV2A is the binding site for the antiepileptic drug levetiracetam. Proc Natl Acad Sci U S A 101: 9861–9866.

Madisen L, et al. (2010) A robust and high-throughput Cre reporting and characterization system for the whole mouse brain. Nat Neurosci 13:133–140.

Marx M, Haas CA, Häussler U (2013) Differential vulnerability of interneurons in the epileptic hippocampus. Front Cell Neurosci 7:57205.

Menten-Dedoyart C, et al. (2016) Development and validation of a new mouse model to investigate the role of SV2A in epilepsy. PLoS One 11:e0166525.

Miri ML, Vinck M, Pant R, Cardin JA (2018) Altered hippocampal interneuron activity precedes ictal onset. Elife 7.

Nakagawa JM, et al. (2017) Characterization of focal cortical dysplasia with balloon cells by layer-specific markers: evidence for differential vulnerability of interneurons. Epilepsia 58:635–645.

Nowack A, Yao J, Custer KL, Bajjalieh SM (2010) SV2 regulates neurotransmitter release via multiple mechanisms. Am J Physiol Cell Physiol 299: C960–C967.

Pack AM (2014) Brivaracetam, a novel antiepileptic drug: is it effective and safe? Results from One Phase III Randomized Trial 14:196–198.
Pathak D, et al. (2015) The role of mitochondrially derived ATP in synaptic vesicle recycling. J Biol Chem 290:22325–22336.
Paul A, et al. (2017) Transcriptional architecture of synaptic communication delineates GABAergic neuron identity. Cell 171:522–539.e20.
Pazarlar BA, et al. (2022) Expression profile of synaptic vesicle glycoprotein 2A, B, and C paralogues in temporal neocortex tissue from patients with temporal lobe epilepsy (TLE). Mol Brain 15:1–10.
Pfisterer U, et al. (2020) Identification of epilepsy-associated neuronal subtypes and gene expression underlying epileptogenesis. Nat Commun 11.
Portela-Gomes GM, Lukinius A, Grimelius L (2000) Synaptic vesicle protein 2, a new neuroendocrine cell marker. Am J Pathol 157:1299–1309.
Ruest LB, Hammer RE, Yanagisawa M, Clouthier DE (2003) Dlx5/6-enhancer directed expression of Cre recombinase in the pharyngeal arches and brain. Genesis 37:188–194.
Russell AJC, et al. (2023) Slide-tags enables single-nucleus barcoding for multimodal spatial genomics. Nature 625:101–109.
Santuy A, et al. (2020) Estimation of the number of synapses in the hippocampus and brain-wide by volume electron microscopy and genetic labeling. Sci Rep 10:1–15.
Schivell AE, Batchelor RH, Bajjalieh SM (1996) Isoform-specific, calcium-regulated interaction of the synaptic vesicle proteins SV2 and synaptotagmin. J Biol Chem 271:27770–27775.
Schivell AE, Mochida S, Kensel-Hammes P, Custer KL, Bajjalieh SM (2005) SV2A and SV2C contain a unique synaptotagmin-binding site. Mol Cell Neurosci 29:56–64.
Scranton TW, Iwata M, Carlson SS (1993) The SV2 protein of synaptic vesicles Is a keratan sulfate proteoglycan. J Neurochem 61:29–44.
Serajee FJ, Huq AM (2015) Homozygous mutation in synaptic vesicle glycoprotein 2A gene results in intractable epilepsy, involuntary movements, microcephaly, and developmental and growth retardation. Pediatr Neurol 52:642–646.e1.
Serrano ME, et al. (2019) Anxiety-like features and spatial memory problems as a consequence of hippocampal SV2A expression. PLoS One 14.
Shi W, et al. (2019) Perineuronal nets protect long-term memory by limiting activity-dependent inhibition from parvalbumin interneurons. Proc Natl Acad Sci U S A 116:27063–27073.
Sommeijer JP, Levelt CN (2012) Synaptotagmin-2 is a reliable marker for parvalbumin positive inhibitory boutons in the mouse visual cortex. PLoS One 7:1–12.
Srinivas S, et al. (2001) Cre reporter strains produced by targeted insertion of EYFP and ECFP into the ROSA26 locus. BMC Dev Biol 1:1–8.
Stenman J, Toresson H, Campbell K (2003) Identification of two distinct progenitor populations in the lateral ganglionic eminence : implications for striatal and olfactory bulb neurogenesis. J Neurosci 23:167–174.
Tai C, Abe Y, Westenbroek RE, Scheuer T, Catterall WA (2014) Impaired excitability of somatostatin- and parvalbumin-expressing cortical interneurons in a mouse model of dravet syndrome. Proc Natl Acad Sci U S A 111.
Takács VT, Szőnyi A, Freund TF, Nyiri G, Gulyás AI (2015) Quantitative ultrastructural analysis of basket and axo-axonic cell terminals in the mouse hippocampus. Brain Struct Funct 220:919–940.
Taniguchi H, et al. (2011) A resource of Cre driver lines for genetic targeting of GABAergic neurons in cerebral cortex. Neuron 71:995–1013.
Toering ST, et al. (2009) Expression patterns of synaptic vesicle protein 2A in elfocal cortical dysplasia and TSC-cortical tubers. Epilepsia 50:1409–1418.
Tokudome K, et al. (2016) A missense mutation of the gene encoding synaptic vesicle glycoprotein 2A (SV2A) confers seizure susceptibility by disrupting amygdalar synaptic GABA release. Front Pharmacol 7:1–10.
Tronche F, et al. (1999) Disruption of the glucocorticoid receptor gene in the nervous system results in reduced anxiety. Nat Genet 23:99–103.
Van Erum J, Van Dam D, De Deyn PP (2019) PTZ-induced seizures in mice require a revised Racine scale. Epilepsy Behav 95:51–55.
Van Vliet EA, Aronica E, Redeker S, Boer K, Gorter JA (2009) Decreased expression of synaptic vesicle protein 2A, the binding site for levetiracetam, during epileptogenesis and chronic epilepsy. Epilepsia 50:422–433.
Vanoye-Carloa A, Gómez-Lirab G (2019) Differential expression of SV2A in hippocampal glutamatergic and GABAergic terminals during postnatal development. Brain Res 1715:73–83.
Venkatesan K, et al. (2012) Altered balance between excitatory and inhibitory inputs onto CA1 pyramidal neurons from SV2A-deficient but not SV2B-deficient mice. J Neurosci Res 90:2317–2327.
Wang D, et al. (2019) Levetiracetam-induced a new seizure type in a girl with a novel SV2A gene mutation. Clin Neurol Neurosurg 181:64–66.
Zamecnik J, et al. (2006) Densities of parvalbumin-immunoreactive neurons in non-malformed hippocampal sclerosis-temporal neocortex and in cortical dysplasias. Brain Res Bull 68:474–481.
Zhang W, et al. (2009) Surviving hilar somatostatin interneurons enlarge, sprout axons, and form new synapses with granule cells in a mouse model of temporal lobe epilepsy. J Neurosci 29:14247–14256.